Anisotropy in the absorption and scattering spectra of chicken breast tissue

Guillermo Marquez, Lihong V. Wang, Shao-Pow Lin, Jon A. Schwartz, and Sharon L. Thomsen

Oblique incidence reflectometry is a simple and accurate method for measuring the absorption and the reduced-scattering coefficients of turbid media. We used this technique to deduce absorption and reduced-scattering spectra from wavelength-resolved measurements of the relative diffuse reflectance profile of white light as a function of source–detector distance. In this study, we measured the absorption and the reduced-scattering coefficients of chicken breast tissue in the visible range (400–800 nm) with the oblique incidence probe oriented at 0° and 90° relative to the muscle fibers. We found that the deduced optical properties varied with the probe orientation. Measurements on homogenized chicken breast tissue yielded an absorption spectrum comparable with the average of the absorption spectra for 0° and 90° probe orientations measured on the unhomogenized tissue. The reduced-scattering spectrum for homogeneous tissue was greater than that acquired for unhomogenized tissue taken at either probe orientation. This experiment demonstrated the application of oblique-incidence, fiber-optic reflectometry to measurements on biological tissues and the effect of tissue structural anisotropy on optical properties.

OCIS codes: 290.0290, 290.7050, 170.6930, 170.7050.

1. Introduction

In this paper, we present the continued research for measuring optical properties of turbid media with oblique-incidence reflectometry. Wang and Jacques[1] first presented this method as a means of measuring the reduced-scattering coefficient of biological tissues at a single wavelength, and Lin *et al.*[2,3] have demonstrated that absorption and reduced-scattering spectra can be easily obtained with this method and with an accuracy of 10% and 5%, respectively. Our current research is aimed at investigating the effect of muscle fiber alignment on optical properties and testing our probe on biological tissues.

It is important to know the optical properties of tissues to dose light delivery properly in therapeutic procedures, such as photocoagulation or photodynamic therapy. Also, the optical properties themselves can potentially provide enough information to monitor tissue metabolic status or diagnose disease, particularly cancer.[4–6] This is because light in the visible and the near infrared interacts with the subcellular components of tissue. Therefore characteristic changes in tissue optical properties at particular wavelengths could be indicative of disease.

Measuring the optical properties, the absorption coefficient (μ_a) and the reduced-scattering coefficient (μ_s'), of biological tissues noninvasively, *in vivo*, and in real time remains a problem in the field of biomedical optics. Other techniques have been developed to measure tissue optical properties. The most common method is the integrating sphere measurement, but this technique requires the removal of a thin slice of tissue and is therefore invasive.[7] Another technique, normal-incidence video reflectometry, provides a noninvasive approach to determine optical properties but requires a measurement of both the spatial distribution of diffuse reflectance and the total diffuse reflectance at each wavelength.[8] Normal-incidence reflectometry has also been implemented with optical fibers.[9,10] In contrast, oblique-incidence reflectometry requires only a measurement of the relative profile of the spatial distribution of diffuse re-

G. Marquez and L. V. Wang (corresponding author) are with the Optical Imaging Laboratory, Biomedical Engineering Program, Texas A&M University, College Station, Texas 77843-3120. S.-P. Lin is with the Neuroscience Program, Washington University School of Medicine, Campus Box 8226, 660 South Euclid Avenue, St. Louis, Missouri 63110. J. A. Schwartz and S. L. Thomsen are with the Laser Biology Research Laboratory, University of Texas M. D. Anderson Cancer Center, 1515 Holcombe Boulevard, Houston, Texas 77030.

Received 2 June 1997; revised manuscript received 2 October 1997.

0003-6935/98/040798-07$10.00/0

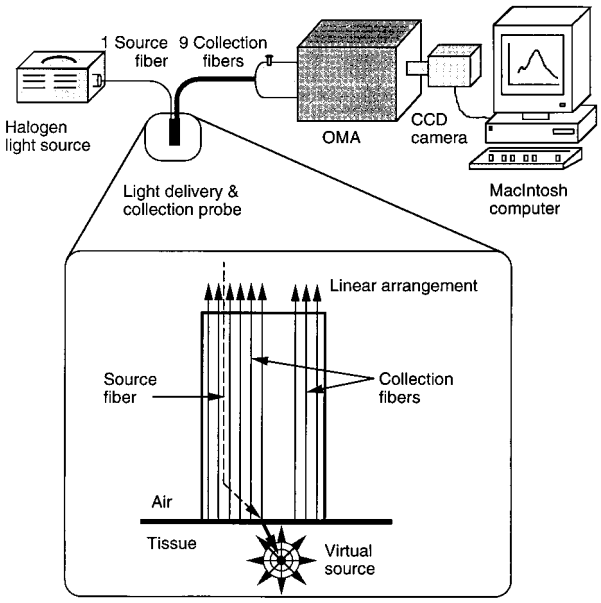

Fig. 1. Schematic of experimental apparatus. White light was coupled to the oblique-incidence optical fiber probe. A source fiber delivered light to the chicken breast tissue at an angle of 45°, and the diffuse reflectance was collected by nine collection fibers. All fibers were encased to form a hand-held probe. The core diameter of the fibers was 600 μm with an index of refraction of 1.46. The index of refraction of chicken breast tissue was 1.37. The angle of refraction was computed to be 48.9°. The collected diffuse reflectance was analyzed and its spectrum recorded with the OMA.

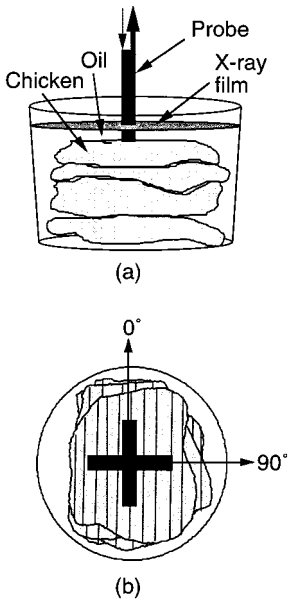

Fig. 2. Chicken breast tissue setup. (a) The container, 10 cm deep and 10 cm in diameter, is shown. The probe makes physical contact with the chicken tissue. Immersion oil is used as a coupling medium. (b) Probe orientation is shown with respect to the muscle fiber orientation: 0° indicates parallel and 90° perpendicular. An exposed x-ray film is placed on top of the chicken tissue to approximate a matched boundary condition for diffusion theory.

flectance. In this paper we used the technique of oblique-incidence reflectometry on chicken skeletal muscle tissue at different angles with respect to the muscle fiber orientation to determine its effect on our deduced tissue optical properties.

2. Methods and Materials

A. Experimental

The experimental system is drawn schematically in Fig. 1. White light (Dolan–Jenner Industries, Fiber-Lite High Intensity Illuminator 170-D) was delivered, and the diffuse reflectance was collected with a fiber-optic probe made from black delrin and 600-μm diameter, low-loss optical fibers. The source fiber was oriented at a 45° angle of incidence, and the nine collection fibers, arranged in a linear array, collected the diffuse reflectance. To correct for slight variations in collection efficiency from one detection fiber to the next, a correction factor was calculated for each fiber based on a calibration procedure with standard phantoms.[2] The detection system was an optical multichannel analyzer (OMA) that utilized a spectrograph (Instruments S.A., HR320), an intensified CCD camera (Princeton Instrument Inc., TRY-700G/RAR/R), and a Macintosh computer to record automatically the spectrum of the collected light through the wavelength range of 400–800 nm.

Frozen, raw, chicken breasts were allowed to thaw at room temperature for 20 min. The skin and fat were removed, and the chicken breasts were cut so as to have only one muscle fiber orientation per piece. The pieces were stacked in a small black container with the muscle fibers aligned [Fig. 2(a)]. The container was then filled with a small amount of microscope immersion oil ($n = 1.5105$) to ensure good coupling between the probe and the chicken breast. An exposed x-ray film was placed on top of the chicken tissue to approximate a matched boundary condition for diffusion theory.[11] Four measurements each were performed with the probe oriented at 0° (parallel) and 90° (perpendicular) relative to the muscle fibers [Fig. 2(b)]. Absorption and reduced-scattering spectra were evaluated for each diffuse reflectance measurement, and the results for each probe orientation were averaged.

After the measurements, all the chicken breasts were blended with a blender until the purée appeared homogeneous by visual inspection. We placed the purée back in the black container making sure no air or oil pockets were created by the blending. Then four measurements at each probe orientation were performed again.

B. Theoretical

In this section we summarize, for completeness, the theory behind our method described in detail by Lin *et al.*[2] When light enters a semi-infinite tissue, it will generally scatter a number of times before either being absorbed or escaping the tissue surface. This scattered light that escapes is called diffuse reflectance. The calculation of absorption coefficient in our method was derived from a diffusion-theory-

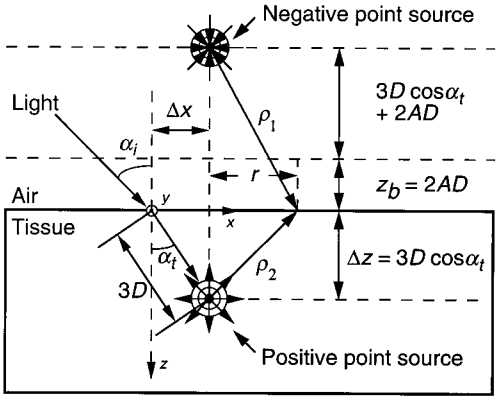

Fig. 3. Schematic representation of obliquely incident light upon a tissue. Note the shift in the center of diffuse reflectance, Δx. The positions of the two point sources in the diffusion-theory model of oblique-incidence reflectometry are shown.

based model of diffuse reflectance,[12] although the calculation of the diffusion constant was independent of diffusion theory.[1,2] This diffusion-theory model does not accurately model near diffuse reflectance, i.e., reflectance that falls within the range of 1–2 transport mean free paths of the source.[13] This problem can be avoided by using only the far diffuse reflectance, i.e., reflectance that falls beyond the range of 1–2 transport mean free path of the source.

For normally incident light, the spatial distribution of diffuse reflectance from a semi-infinite turbid medium has been modeled by two isotropic point sources: one positive source located below the tissue surface and one negative image source above the tissue surface.[12] If light is delivered obliquely, the positive source is buried at the same distance from the point of incidence but with a depth modified by Snell's law. Wang and Jacques[1] found the distance of the buried source to the point of incidence to be most accurately determined by

$$3D = \frac{1}{0.35\mu_a + \mu_s'}, \tag{1}$$

where D is defined as the diffusion coefficient,[2] μ_a the absorption coefficient, and μ_s' the reduced-scattering coefficient. Therefore the fundamental difference between normal- and oblique-incidence is a shift in the positions of the point sources in the x direction (Fig. 3). This shift, Δx, is

$$\Delta x = \frac{\sin(\alpha_i)}{n(0.35\mu_a + \mu_s')} = \frac{\sin(\alpha_t)}{0.35\mu_a + \mu_s'}, \tag{2}$$

where n is the relative index of refraction, α_i is the angle of incidence, and α_t is the angle of refraction. The relative index of refraction is unity for a matched boundary.

The modified dipole source diffusion-theory model gives diffuse reflectance

$$R(x) = \frac{\Delta z(1 + \mu_{\text{eff}}\rho_1)\exp(-\mu_{\text{eff}}\rho_1)}{4\pi\rho_1^3} + \frac{(\Delta z + 2z_b)(1 + \mu_{\text{eff}}\rho_2)\exp(-\mu_{\text{eff}}\rho_2)}{4\pi\rho_2^3}, \tag{3}$$

where ρ_1 and ρ_2 are the distances from the two point sources to the point of interest, z_b is the distance between the virtual boundary and the surface of the tissue,

$$z_b = 2AD, \tag{4}$$

where A is unity for a matched boundary, Δz is the depth of the positive point source,

$$\Delta z = \frac{\cos(\alpha_t)}{0.35\mu_a + \mu_s'} = \Delta x \tan^{-1}(\alpha_t), \tag{5}$$

and μ_{eff} is the effective attenuation coefficient

$$\mu_{\text{eff}} = (\mu_a/D)^{1/2}. \tag{6}$$

Equation (3) can be scaled to fit a relative reflectance profile.

Therefore the first step in our procedure was to measure the diffuse reflectance profile with our fiber-optic probe. We used white light for a multiwavelength measurement. The light collected by each detection fiber was input to the OMA for spectral resolution. Because we determine the spectrum collected by each fiber, we have in fact measured the spatial distribution of diffuse reflectance at many wavelengths simultaneously [Fig. 4(a)]. Thus the reflectance profile at any wavelength can be extracted and analyzed to deduce the optical properties at that wavelength [Fig. 4(b)].

Once the position of the center of far diffuse reflectance relative to the light entry point (Δx) was found, the diffusion coefficient was calculated from

$$D = \frac{\Delta x}{3\sin(\alpha_t)}. \tag{7}$$

Then a nonlinear least-squares fit to Eq. (3) with the Levenberg–Marquardt method[14] yielded the effective attenuation coefficient, μ_{eff}. Equations (1), (2), and (6) were used to compute μ_a and μ_s' as follows:

$$\mu_a = \frac{\mu_{\text{eff}}^2\Delta x}{3\sin(\alpha_t)}, \tag{8}$$

$$\mu_s' = \frac{\sin(\alpha_t)}{\Delta x} - 0.35\mu_a. \tag{9}$$

3. Results

As shown in Fig. 5, we could measure the full visible spectrum of the average absorption coefficient (μ_a) and reduced-scattering coefficient (μ_s') for both probe orientations. In Fig. 5(a), we also included the scaled absorption coefficient of deoxyhemoglobin for

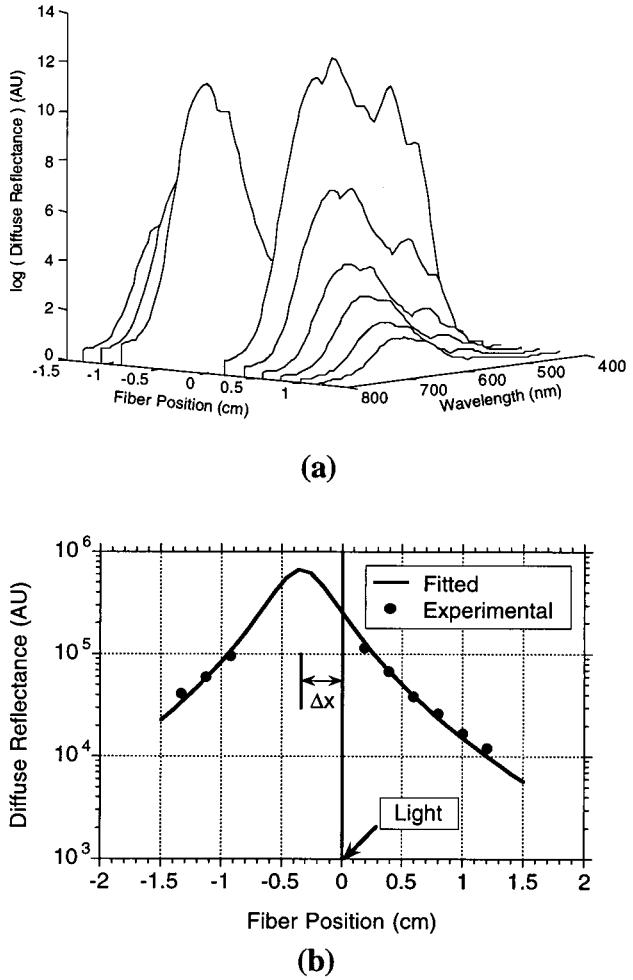

Fig. 4. (a) Spectra of the spatially distributed diffuse reflectance between 400 and 800 nm of chicken breast tissue with the fiber probe oriented at 0° with respect to the muscle fiber orientation. Each line on the figure represents the spectrum collected by one of the nine collection fibers. There were no detection fibers between −0.92 and +0.19 cm. (b) Example of one spectral slice at 632.4 nm through our chicken tissue data at 0° probe orientation relative to the muscle fiber orientation. Note the obliquely incident light and the shift in the center of diffuse reflectance, Δx.

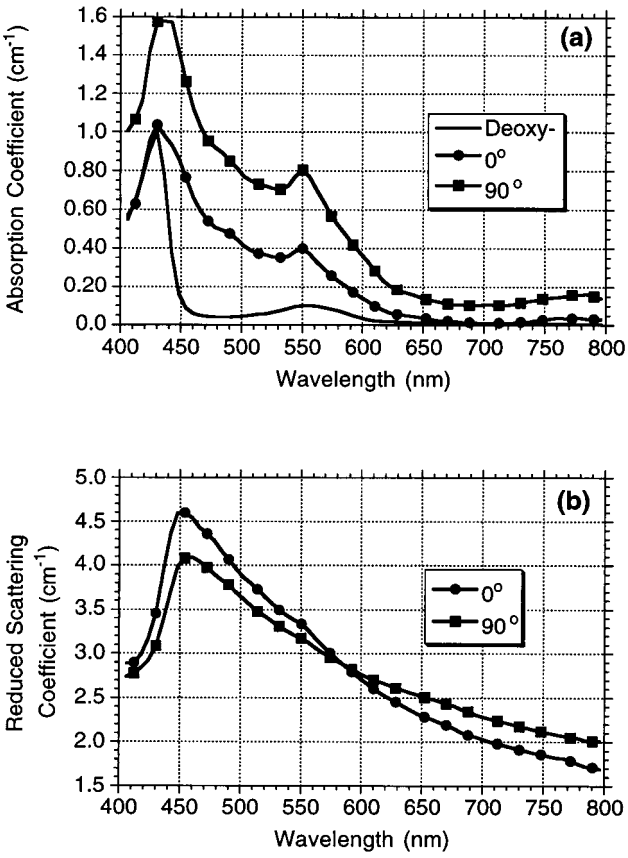

Fig. 5. (a) Absorption spectra of chicken breast tissue with the probe aligned at 0° (parallel) and 90° (perpendicular) with respect to the muscle fiber orientation. The absorption spectrum of deoxyhemoglobin is also plotted. The values for deoxyhemoglobin are relative; its use in this graph is to show its similarities with our measured absorption spectra. (b) The reduced-scattering spectra with the probe aligned at 0° and 90° with respect to the muscle fiber orientation. The coefficient decreased smoothly with increase in wavelength beyond a peak at approximately 450 nm.

comparison. Two peaks at approximately 430 and 550 nm were observed in all three absorption curves. The absorption coefficient was consistently lower at 0° than that at 90°. The reduced-scattering coefficient curves peaked at approximately 450 nm, then decreased smoothly with increasing wavelength [Fig. 5(b)]. The 90° curve had a lower μ_s' than the 0° curve below the crossover wavelength at approximately 585 nm.

The average absorption and reduced-scattering coefficients for the homogenized chicken tissue are plotted in Fig. 6. Figure 6(a) shows two absorption peaks at 430 and 540 nm, and Fig. 6(b) shows a reduced-scattering coefficient peak at the 450-nm wavelength. The absorption coefficient of the homogenized chicken tissue was approximately equal to the average of the absorption coefficients for 0° and 90° probe orientations. We also found that the reduced-scattering coefficient for homogenized tissue was higher than that for either 0° or 90° probe orientation.

Figure 7 shows the average absorption and reduced-scattering coefficients at 0° for two different samples. The absorption and the reduced-scattering coefficients varied from sample to sample. However, the patterns seen in Fig. 5 held for each independent sample.

4. Discussion and Conclusions

Oblique-incidence reflectometry can quickly, inexpensively, and noninvasively measure the absorption and the reduced-scattering coefficients of turbid media. We accomplished the multiwavelength measurements by replacing a monochromatic light source with a white-light source. In our experiments, we used chicken breast as a prelude to clinical studies. We hoped to determine the effect of anisotropically structured media, such as muscle, on the optical properties of tissues. Chicken breast was chosen because it has good muscle orientation, can be virtually fat-free, and may be consistently prepared.

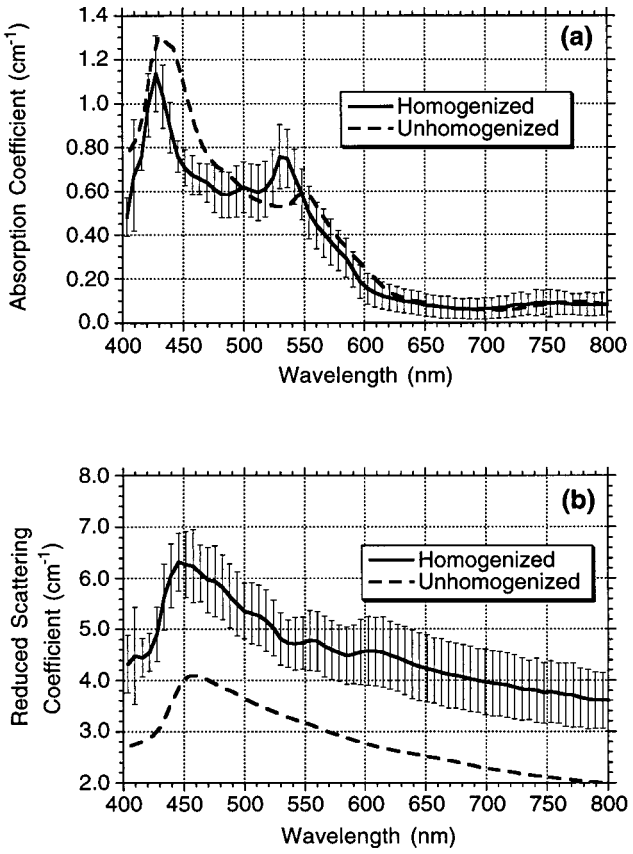

Fig. 6. (a) Absorption coefficient spectrum for homogenized chicken tissue was approximately equal to the average of the absorption coefficients for 0° and 90° probe orientation. (b) The reduced-scattering coefficient spectrum for homogenized chicken breast tissue was greater than those for either 0° or 90° probe orientation.

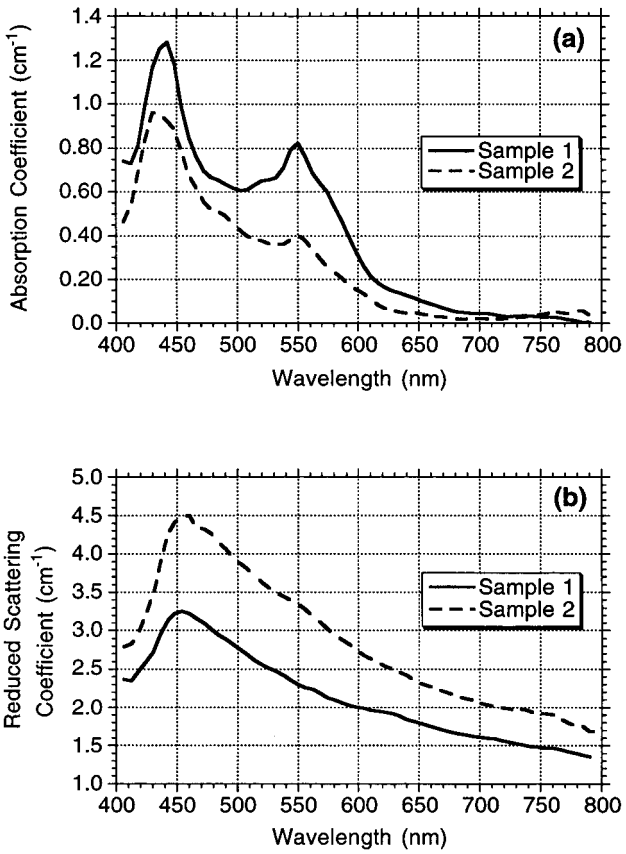

Fig. 7. (a) Absorption coefficient at 0° probe orientation with respect to muscle fiber orientation for two different samples of chicken breast tissue. (b) Reduced-scattering coefficient at 0° probe orientation with respect to muscle fiber orientation for the two samples. There was variability in absolute values between samples; however, the patterns persisted.

Note that the minimal observed absorption coefficient was 0.06 cm^{-1} and that the minimal reduced-scattering coefficient was 1.5 cm^{-1}. The corresponding maximum penetration depth was 1.9 cm. Therefore the 10-cm dimension of the container was much greater than the penetration depth, and the tissue sample may be considered semi-infinite as assumed in the theoretical modeling of the diffuse reflectance.

As shown in Fig. 5, there were differences in the absorption and the reduced-scattering coefficients due to changes in the probe orientation. The absorption and the reduced-scattering coefficients had an average of 17% and 6% error, respectively, for both probe orientations. An interesting observation was that our absorption spectra matched the peaks of the previously published deoxyhemoglobin absorption spectrum [Fig. 5(a)]. The double peaks in the measured absorption spectra should be caused by some residual hemoglobin in the chicken breast tissue. Since the measured peak absorption coefficients were not proportional to the corresponding peaks of hemoglobin, there must be some other absorbers in the chicken muscle tissue that had contributed to the absorption spectra. It was unclear to what extent the effect of myoglobin was present in the measured absorption spectra. However, myoglobin has absorption maxima for horses at 435 and 560 nm and for whales at 434 and 556 nm and probably had contributed to the spectrum also.[15]

The reduced-scattering spectra showed a peak at 450 nm. The slope of the reduced-scattering coefficient above 450 nm was related to Rayleigh scattering for which the wavelength was much greater than the dimension of the scatterers. The slope below 450 nm was a result of the wavelength being comparable with the dimension of the scatterers. The scattering coefficient, calculated with the Mie theory for spherical scatterers,[16,17] oscillated when the particle size became comparable to the wavelength. Although the scatterers in chicken muscle tissue cannot be considered as spherical particles, the Mie theory helped in understanding the deviation of the reduced-scattering coefficient from the monotonic increase with decreasing wavelength.

The anisotropy in the measured absorption and reduced-scattering coefficients was related to the structural anisotropy in the chicken breast tissue caused by the alignment of muscle fibers. The relative difference in the measured absorption coeffi-

cients between the 0° and the 90° probe orientations was as much as 50%. The lower absorption coefficient at 0° than that at 90° was probably caused by the light-guiding effect of the muscle fibers. The space between the muscle fibers is occupied by blood capillaries of greater absorption. The percentage of the optical path inside the muscle fibers when the probe was parallel with the muscle fibers was probably greater than that when the probe was perpendicular, and led to a lower absorption coefficient. Since the extraction of absorption coefficient depended on diffusion theory for isotropic media, the anisotropy in the absorption spectra may have been caused by the diffusion theory. A more sophisticated model dealing with anisotropic media should be used to determine the absorption from the experimental data more precisely and would yield a decisive conclusion. The traditional Monte Carlo method[18,19] can be extended to simulate anisotropic turbid media following the theoretical work for other media.[20]

The relative difference in the measured reduced-scattering coefficients between the 0° and the 90° probe orientations was as much as 10%. The birefringence effect of the structural anisotropy is well known[21] but does not explain the large anisotropy in the absorption and the reduced-scattering coefficients because the light source and the detection system in our experimental system were unpolarized. However, the striated structure of the chicken muscle tissue was expected to cause different scattering properties along and perpendicular to the muscle fibers. The Mie theory for cylindrical scattering particles[22] may provide a modeling avenue for this anisotropic scattering problem.

We blended the chicken sample to compare the results obtained from structurally anisotropic tissues with those from a homogeneous sample of the same chicken tissue (Fig. 6). The absorption spectrum for homogenized chicken tissue was approximately equal to the average of the absorption spectra for 0° and 90° probe orientation. The blue shift of the absorption peaks in the homogenized muscle tissue reflected the oxygenation of hemoglobin and possibly myoglobin during the homogenization procedure[23] in which the chicken tissue purée presented more tissue surfaces to the ambient air, resulting in the binding of oxygen.

The reduced-scattering spectrum for homogenized chicken breast tissue was greater than that for either 0° or 90° probe orientation, which was caused by the many added interfaces among the fragments of muscle and collagen created by blending the chicken tissue. The standard deviations in the measured absorption and reduced-scattering coefficients of homogenized tissue were approximately twice as much as those for the unhomogenized tissue and were presented as error bars in Fig. 6. The greater errors may have been caused by the rough tissue surface in the homogenized form.

The optical properties of chicken tissue vary from sample to sample (Fig. 7). However, similar patterns and peaks persisted between different chicken samples. The differences in the coefficients most likely were due to biological variations and/or preparation, such as prolonged freezing and thawing times that can lead to cell rupture.

Our algorithm to fit for the absorption coefficient was based on the diffusion theory for the propagation of light in a structurally isotropic media. Since chicken breast tissue was not an isotropic medium, our absorption measurements were somewhat approximate. However, the reduced-scattering coefficient was accurate since Eq. (9) was not based on the diffusion theory and the contribution from the absorption coefficient to the right side of Eq. (9) was insignificant. By comparison, normal-incidence reflectometry that has been developed so far is unable to detect the anisotropy in tissue optical properties.

In conclusion, this research has demonstrated the application of oblique-incidence fiber-optic reflectometry to measurements on biological tissues and the effect of structural anisotropy on the deduced optical properties. The relative difference in the measured absorption coefficients between the 0° and the 90° probe orientations was as much as 50% and that in the measured reduced-scattering coefficients was as much as 10%. The anisotropic properties of some tissues will affect light-tissue interaction in both diagnostic and therapeutic aspects. Modeling with the anisotropic optical properties of tissues will more accurately simulate light propagation in the anisotropic tissues.

We give special thanks to J. T. Connor and S. K. Martin for their contributions to this project. The project was sponsored in part by The Whitaker Foundation grant and the National Institutes of Health grants R29 CA68562 and R01 CA71980.

References and Notes

1. L.-H. Wang and S. L. Jacques, "Use of a laser beam with an oblique angle of incidence to measure the reduced scattering coefficient of a turbid medium," Appl. Opt. **34,** 2362–2366 (1995).
2. S.-P. Lin, L.-H. Wang, S. L. Jacques, and F. K. Tittel, "Measurement of tissue optical properties by the use of oblique-incidence optical fiber reflectometry," Appl. Opt. **36,** 136–143 (1997).
3. S.-P. Lin, L.-H. Wang, S. L. Jacques, and F. K. Tittel, "Measurement of absorption and scattering spectra with oblique incidence reflectometry," in *Biomedical Optical Spectroscopy and Diagnostics*, E. Sevick-Muraca and D. Benaron, eds., Vol. 3 of OSA Trends in Optics and Photonics Series (Optical Society of America, Washington, D.C., 1996), pp. 44–49.
4. D. Benaron, G. Mueller, and B. Chance, "Introduction: a medical perspective at the threshold of clinical optical tomography," in *Medical Optical Tomography: Functional Imaging and Monitoring*, G. Mueller, ed., Vol. 11 of 1993 SPIE Institutes (Society of Photo-Optical Instrumentation Engineers, Bellingham, Wash., 1993), pp. 3–9.
5. R. Marchesini, M. Brambilla, C. Clemente, M. Maniezzo, A. E. Sichirollo, A. Testori, D. R. Venturoli, and N. Casinelli, "*In vivo* spectrophotometric evaluation of neoplastic and non-neoplastic skin pigmented lesions—I. Reflectance measurements," Photochem. Photobiol. **53,** 77–84 (1991).
6. R. Marchesini, N. Casinelli, M. Brambilla, C. Clemente, L. Mascheroni, E. Pignoli, A. Testori, and D. R. Venturoli, "*In vivo* spectrophotometric evaluation of neoplastic and non-

neoplastic skin pigmented lesions—II. Discriminant analysis between nevus and melanoma," Photochem. Photobiol. **55,** 515–522 (1992).
7. J. W. Pickering, S. A. Prahl, N. Vanwieringen, J. F. Beek, H. J. C. M. Sterenborg, and M. J. C. van Gemert, "Double-integrating-sphere system for measuring the optical properties of tissue," Appl. Opt. **32,** 399–410 (1993).
8. S. L. Jacques, A. Gutsche, J. A. Schwartz, L.-H. Wang, and F. K. Tittel, "Video reflectometry to extract optical properties of tissue *in vivo*," in *Medical Optical Tomography: Functional Imaging and Monitoring*, G. Mueller, ed., Vol. **11** of SPIE Institutes (Society of Photo-Optical Instrumentation Engineers, Bellingham, Wash., 1993), pp. 211–226.
9. T. J. Farrell, B. C. Wilson, and M. S. Patterson, "The use of a neural network to determine tissue optical properties from spatially resolved diffuse reflectance measurements," Phys. Med. Biol. **37,** 2281–2286 (1992).
10. M. G. Nichols, E. L. Hull, and T. H. Foster, "Design and testing of a white-light, steady-state diffuse reflectance spectrometer for determination of optical properties of highly scattering systems," Appl. Opt. **36,** 93–104 (1997).
11. S.-P. Lin, "Oblique-incidence fiber-optic reflectometry for measuring absorption and scattering in turbid media," M. S. thesis (Rice University, Houston, Tex., 1996).
12. T. J. Farrell, M. S. Patterson, and B. C. Wilson, "A diffusion theory model of spatially resolved, steady-state diffuse reflectance for the non-invasive determination of tissue optical properties *in vivo*," Med. Phys. **19,** 879–888 (1992).
13. L.-H. Wang and S. L. Jacques, "Analysis of diffusion theory and similarity relations," in *Photon Migration and Imaging in Random Media and Tissues*, B. Chance and R. R. Alfano, eds., Proc. SPIE **1888,** 107–116 (1993).
14. W. H. Press, B. P. Flannery, S. A. Teukolsky, and W. T. Vetterlin, *Numerical Recipes in C*, 2nd ed. (Cambridge U., Cambridge, UK, 1992), Section 15.5.
15. E. Antonini and M. Brunori, *Hemoglobin and Myoglobin and their Reactions with Ligands* (Elsevier, New York, 1971), pp. 16–20.
16. M. Born and E. Wolf, *Principles of Optics: Electromagnetic Theory of Propagation, Interference and Diffraction of Light*, 6th (corrected) ed. (Pergamon, New York, 1986), Section 13.5.
17. C. F. Bohren and D. R. Huffman, *Absorption and Scattering of Light by Small Particles* (Wiley, New York, 1983).
18. L.-H. Wang, S. L. Jacques, and L.-Q. Zheng, "MCML—Monte Carlo modeling of photon transport in multi-layered tissues," Comput. Meth. Programs Biomed. **47,** 131–146 (1995). The MCML/CONV software package may be downloaded from http://biomed.tamu.edu/~lw.
19. L.-H. Wang, S. L. Jacques, and L.-Q. Zheng, "CONV—Convolution for responses to a finite diameter photon beam incident on multi-layered tissues," Comput. Meth. Programs Biomed. **54,** 141–150 (1997).
20. H. Stark, M. H. Kao, K. A. Jester, T. C. Lubensky, and A. G. Yodh, "Light diffusion and diffusing-wave spectroscopy in nematic liquid crystals," J. Opt. Soc. Am. A. **14,** 156–178 (1997).
21. P. T. Tran, S. Inoue, E. D. Salmon, and R. Oldenbourg, "Muscle fine structure and microtubule birefringence measured with a new pol-scope," Biol. Bull. **187,** 244–245 (1994).
22. H. C. van de Hulst, *Light Scattering by Small Particles* (Dover, New York, 1981).
23. E. Chan, T. Menovsky, and A. J. Welch, "Effects of cryogenic grinding on soft-tissue optical properties," Appl. Opt. **35,** 4526–4532 (1996).